Is the Critical Role of Loop 3 of *Escherichia coli* 6-Hydroxymethyl-7,8-dihydropterin Pyrophosphokinase in Catalysis Due to Loop-3 Residues Arginine-84 and Tryptophan-89? Site-Directed Mutagenesis, Biochemical, and Crystallographic Studies[†,‡]

Yue Li,[§,||] Jaroslaw Blaszczyk,[||,⊥,#] Yan Wu,[§] Genbin Shi,[§] Xinhua Ji,[*,⊥] and Honggao Yan[*,§]

Department of Biochemistry and Molecular Biology, Michigan State University, East Lansing, Michigan 48824, and Macromolecular Crystallography Laboratory, National Cancer Institute, Post Office Box B, Frederick, Maryland 21702

Received February 24, 2005; Revised Manuscript Received April 27, 2005

ABSTRACT: Deletion mutagenesis, biochemical, and X-ray crystallographic studies have shown that loop 3 of *Escherichia coli* 6-hydroxymethyl-7,8-dihydropterin pyrophosphokinase (HPPK) is required for the assembly of the active center, plays an important role in the stabilization of the ternary complex of HPPK with MgATP and 6-hydroxymethyl-7,8-dihydropterin (HP), and is essential for catalysis. Whether the critical functional importance of loop 3 is due to the interactions between residues R84 and W89 and the two substrates has been addressed by site-directed mutagenesis, biochemical, and X-ray crystallographic studies. Substitution of R84 with alanine causes little changes in the dissociation constants and kinetic constants of the HPPK-catalyzed reaction, indicating that R84 is not important for either substrate binding or catalysis. Substitution of W89 with alanine increases the K_d for the binding of MgATP by a factor of 3, whereas the K_d for HP increases by a factor of 6, which is due to the increase in the dissociation rate constant. The W89A mutation decreases the rate constant for the chemical step of the forward reaction by a factor of 15 and the rate constant for the chemical step of the reverse reaction by a factor of 25. The biochemical results of the W89A mutation indicate that W89 contributes somewhat to the binding of HP and more significantly to the chemical step. The crystal structures of W89A show that W89A has different conformations in loops 2 and 3, but the critical catalytic residues are positioned for catalysis. When these results are taken together, they suggest that the critical functional importance of loop 3 is not due to the interactions of the R84 guanidinium group or the W89 indole ring with the substrates.

6-Hydroxymethyl-7,8-dihydropterin pyrophosphokinase (HPPK)[1] catalyzes the transfer of pyrophosphate from ATP to 6-hydroxymethyl-7,8-dihydropterin (HP, Figure 1a), leading to the biosynthesis of folate cofactors (*1*). Folate cofactors are essential for life (*2*). Mammals have an active transport system for deriving folates from their diet. In contrast, most microorganisms must synthesize folates *de novo* because they lack the active transport system. Therefore, like other enzymes in the folate biosynthetic pathway, HPPK is an attractive target for developing antimicrobial agents.

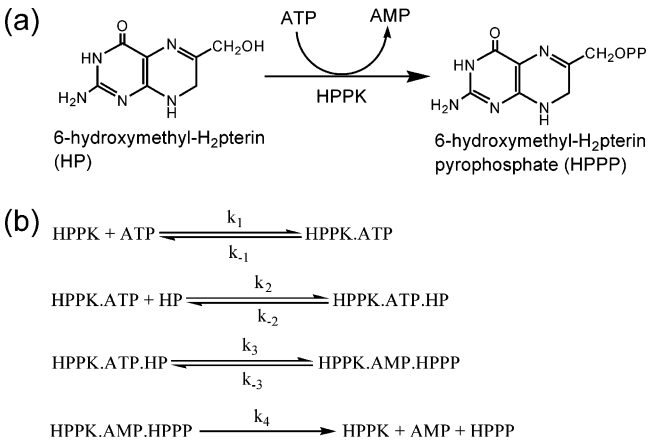

FIGURE 1: Pyrophosphoryl transfer reaction catalyzed by HPPK (a) and its kinetic mechanism (b). Mg^{2+} is required for the reaction, but for simplicity, Mg^{2+} is not shown in the kinetic scheme.

HPPK has also emerged as an excellent model for studying the role of protein dynamics in enzymatic catalysis, because the enzyme is small (158 residues, ~18 kDa), stable, monomeric, and amenable to both X-ray crystallographic and NMR analysis. Atomic structures have been determined for nearly every stage of the catalytic cycle, and protein dynamics has been shown to be important for HPPK catalysis (*3*−*14*).

[†] This work was supported in part by NIH Grant GM51901 (to H.Y.).
[‡] The coordinates and structure factors have been deposited in the Protein Data Bank with the accession codes 1TMJ for apo W89A and 1TMM for W89A·MgAMPCPP·HP.

* To whom correspondence should be addressed. Telephone: (517) 353-8786 (H.Y.); (301) 846-5035 (X.J.). Fax: (517) 353-9334 (H.Y.); (301) 846-6073 (X.J.). E-mail: yanh@msu.edu (H.Y.); jix@ncifcrf.gov (X.J.).
[§] Michigan State University.
[||] These authors contributed equally to this work.
[⊥] National Cancer Institute.
[#] Current address: Michigan State University.

[1] Abbreviations: AMPCPP, α,*β*-methyleneadenosine triphosphate; Ant-ATP, 3′(2′)-*O*-anthraniloyladenosine 5′-triphosphate; GST, glutathione *S*-transferase; HPPK, 6-hydroxymethyl-7,8-dihydropterin pyrophosphokinase; HP, 6-hydroxymethyl-7,8-dihydropterin; NTP, nucleoside triphosphate; HPO, 6-hydroxymethylpterin; rmsd, root-mean-square deviation.

10.1021/bi0503495 CCC: $30.25
Published on Web 05/25/2005

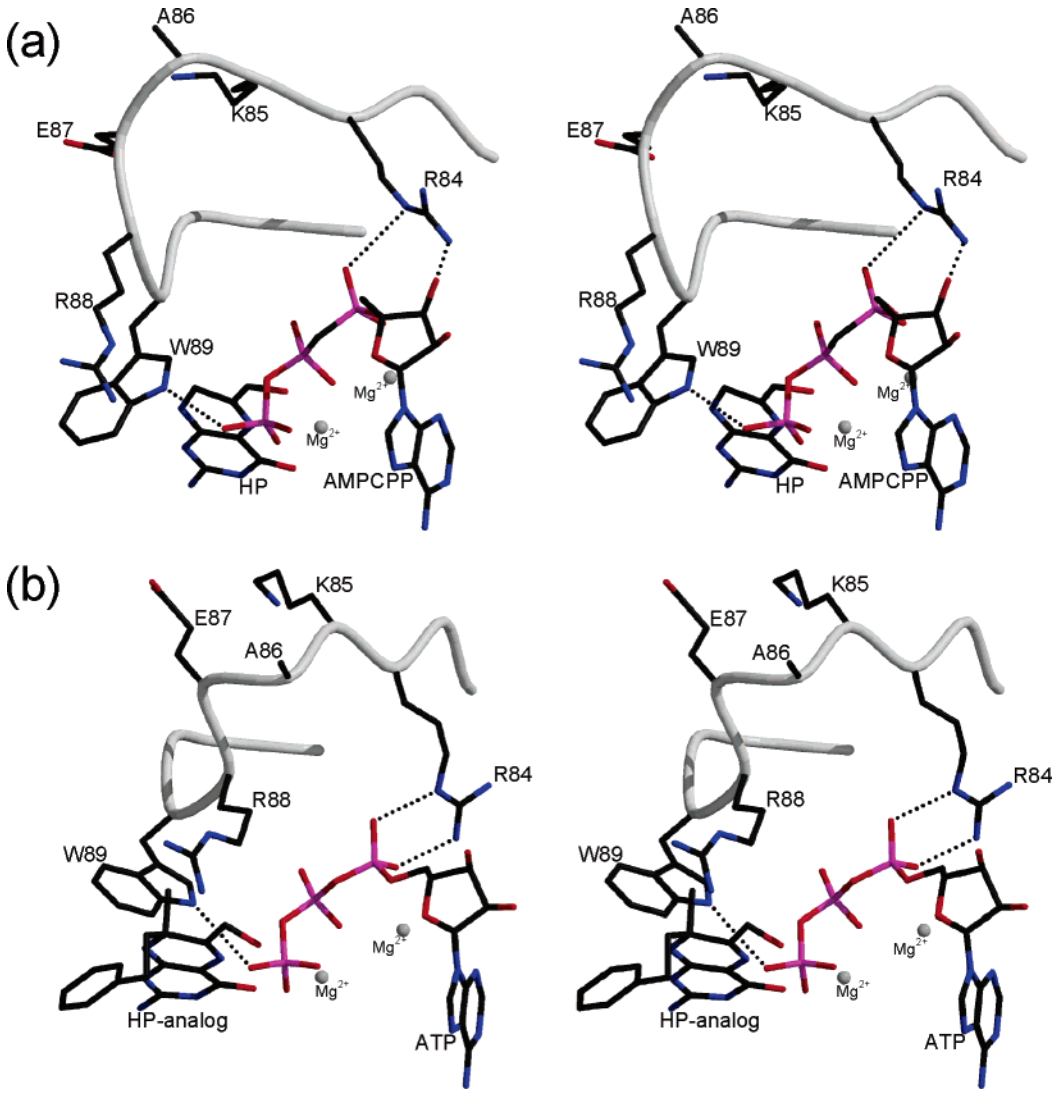

FIGURE 2: Stereoview showing the interactions of HPPK loop 3 with substrates and substrate analogues. (a) Interactions of the loop with HP and an ATP analogue [PDB accession code 1Q0N (*6*)]. (b) Interactions of the loop with ATP and an HP analogue [PDB accession code 1DY3 (*5*)]. Loop 3 is illustrated as a gray pipe. The side chains of loop residues, substrates, and substrate analogues are shown as stick models in atomic color scheme (carbon in black, nitrogen in blue, oxygen in red, and phosphorus in pink). The Mg^{2+} ions are represented by gray spheres, and hydrogen bonds are represented by dotted lines. The figure was prepared with MolScript (*25*) and Raster3D (*26*).

Comparative analysis of the crystal structures of ligand-free HPPK and its ternary complex has revealed that the complete active center of HPPK is assembled only after both substrates bind to the enzyme (*6*). The assembling of the active center involves large substrate-induced conformational changes, particularly in three catalytic loops. Of the three catalytic loops, loop 3 undergoes the most dramatic conformational changes. As expected, the loop moves in to close the active center upon the formation of the ternary complex (*6*). However, the loop moves away from the active center upon the binding of MgADP or an MgATP analogue (*9*). Recently, we have shown that loop 3 also moves away from the active center upon the completion of pyrophosphoryl transfer, to the same extend as upon the binding of MgADP or an MgATP analogue (*14*). Therefore, the unusual conformation of loop 3 appears to be an intermediate required for both MgATP binding and product release during the catalytic cycle.

Loop 3 connects α-helix 2 (α2) and *β*-strand 4 (*β*4) and is delimited by two strictly conserved arginine residues, R82 at its N terminus and R92 at its C terminus (*5*, *6*). We have shown that both R82 and R92 play important roles in catalysis (*11*, *12*). By deletion mutagenesis, we have also shown that the loop connecting R82 and R92 is required for the assembly of the full active center, plays an important role in the stabilization of the ternary complex and the transition state of the reaction, and is essential for catalysis (*13*). However, whether the functional importance of loop 3 is due to the interactions of residues in the loop with the substrates has not been resolved. As revealed by X-ray crystallography, in addition to R82 and R92, which were preserved in the deletion mutant, the only residues on loop 3 that are within 4 Å of the bound substrate and substrate analogue are R84 and W89. The side chains of R84 and W89 undergo dramatic conformational changes and have several interactions with the substrate and substrate analogue. In the crystal structure of HPPK in complex with HP, Mg^{2+}, and ATP analogue α,*β*-methyleneadenosine triphosphate (AMPCPP) [PDB accession code 1Q0N (*6*), HPPK·MgAMPCPP·HP], the guanidinium group of R84 is hydrogen-bonded to the α phosphate and 3′-hydroxyl group of the nucleotide and the indole ring of W89 is hydrogen-bonded to the *γ* phosphate of the

nucleotide and covers one edge of the bound HP (Figure 2a). In the crystal structure of HPPK in complex with ATP, Mg^{2+}, and an HP analogue [PDB accession code 1DY3 (*5*), HPPK·MgATP·HP analogue], the guanidinium group of R84 is hydrogen-bonded to two oxygen atoms of the α phosphate of ATP and the indole ring of W89 is hydrogen-bonded to the γ phosphate of ATP and covers one edge of the bound HP as in the other ternary complex (Figure 2b). To further examine the functional role of loop 3 and particularly the roles of R84 and W89 in HPPK catalysis, we have replaced R84 and W89 individually with alanines and carried out biochemical and X-ray crystallographic studies. Our results suggest that R84 is not important for either substrate binding or catalysis, W89 contributes somewhat to the binding of HP and more significantly to the chemical step, and the critical role of loop 3 in catalysis is not due to the interactions of the guanidinium group of R84 or the indole ring of W89 with the substrates.

EXPERIMENTAL PROCEDURES

Materials. ATP and AMPCPP were purchased from Sigma. 6-Hydroxymethylpterin (HPO) was synthesized according to Thijssen (*15*) and had the same UV absorption and NMR spectra as that purchased from Sigma. HP was prepared from HPO by reduction with sodium dithionite (*16*) or purchased from Schircks Laboratories.

Mutant Construction and Protein Purification. Both mutants were made by a PCR-based method using high-fidelity *pfu* DNA polymerase according to a protocol developed by Stratagene. The forward and reverse primers for making the mutants were 5′-CAGCAAGGTCGCGTC-GCCAAA GCTGAACGCTGG-3′ and 5′-CCAGCGTTC-AGCTTTGGCGACGCGACCTTGCTG-3′ for R84A and 5′-CGCAAAGCTGAACGCGCGGGACCACGCACG-3′ and 5′-CGTGCGTGGTCCCGCGCGTTCAGCTTTGCG-3′ for W89A. The mutants were selected by DNA sequencing. To ensure that there were no unintended mutations in the mutants, the entire sequences of the mutated genes were determined. The mutant proteins were purified as previously described for the wild-type enzyme (*7*).

Construction and Purification of HPPK-Glutathione S-Transferase (GST) Fusion Proteins. The gene for R84A or W89A was subcloned into the *Nde* I and *Bam*H I sites of a homemade expression vector (pET14b-3T) derived from the Novagen vector pET14b. The mutant protein was fused to GST with a link that included a thrombin cleavage site. The fusion protein was purified with a glutathione agarose column and digested with thrombin. The thrombin-digested proteins were run through a Sephadex G-75 column. The HPPK fractions were located by SDS−PAGE and concentrated by an Amicon cell with a YM10 membrane disk.

Thermodynamic Analysis. The K_d values for various ligands were measured by fluorometric titration at 24 °C on a Spex FluoroMax-2 fluorometer as previously described (*7*, *10*). The titration experiments were performed in a single cuvette so that both protein and ligand concentrations varied with the addition of each aliquot of a stock solution. The independent variable in such an experiment was the volume of the added stock solution. To determine the dissociation constant of Ant-ATP, 3 μM R84A or W89A was titrated with Ant-ATP in 100 mM Tris-HCl and 10 mM $MgCl_2$ at pH 8.3. The excitation wavelength and slit were 370 and 1 nm, respectively. The emission wavelength and slit were 425 and 5 nm, respectively. A set of control data was obtained in the absence of the protein. The data obtained in the absence of the protein were then subtracted from the corresponding data set obtained in the presence of the protein after correcting inner-filter effects. The dissociation constant for Ant-ATP was obtained by a nonlinear least-squares fit of the subtracted data (*7*).

The dissociation constants for nonfluorescent nucleotides were measured by a competitive binding assay as previously described (*10*). Briefly, a solution containing 10 μM enzyme and 10 μM Ant-ATP in 100 mM Tris-HCl and 10 mM $MgCl_2$ at pH 8.3 was titrated with ATP or AMPCPP. The excitation wavelength and slit were 337 and 1 nm, respectively. The emission wavelength and slit were 425 and 5 nm, respectively. The fluorometric data was fitted by the nonlinear least-squares method (*10*).

To determine the K_d value for HP, a solution containing 0.55 μM HP and 200 μM AMPCPP in 50 mM BICINE, 10 mM $MgCl_2$, and 25 mM DTT at pH 8.3 was titrated with R84A or W89A (*10*). The excitation wavelength and slit were 330 and 5 nm, respectively. The emission wavelength and slit were 430 and 10 nm, respectively. A control titration experiment was performed in the absence of HP. The control data set obtained in the absence of HP was subtracted from the corresponding data set obtained in the presence of HP. The data were then analyzed by the nonlinear least-squares method (*10*).

Stopped-Flow Analysis. Stopped-flow experiments were performed in an Applied Photophysics SX.18MV-R stopped-flow spectrofluorometer as previously described (*10*). To measure the binding of MgATP to R84A, a solution containing the mutant protein was mixed rapidly with a solution containing ATP and $MgCl_2$ at 25 °C. Fluorescence traces were obtained with an excitation wavelength of 295 nm and a filter with a cutoff of 320 nm for emission. The mutant protein and $MgCl_2$ were fixed at 2 μM and 10 mM, respectively. ATP was varied from 4 to 40 μM.

To measure the binding of MgAMPCPP, a solution containing R84A or W89A was mixed rapidly with a solution containing AMPCPP, $MgCl_2$, and HP at 25 °C. Fluorescence traces were obtained with an excitation wavelength of 340 nm and a filter with a cutoff of 395 nm for emission. The mutant protein, HP, and $MgCl_2$ were fixed at 1 μM, 20 μM, and 10 mM, respectively. AMPCPP was varied from 5 to 30 μM.

To measure the binding of HP, a solution containing the mutant protein, AMPCPP, and $MgCl_2$ was mixed rapidly with a solution containing HP at 25 °C. Fluorescence traces were obtained with an excitation wavelength of 330 nm and a filter with a cutoff of 395 nm for emission. HP, AMPCPP, and $MgCl_2$ were fixed at 1 μM, 30 μM, and 10 mM, respectively. The mutant protein was varied from 2 to 16 μM. All concentrations referred to the concentrations right after the rapid mixing. The rate constants were evaluated by numerical analysis of the stopped-flow data using DYNAFIT (*17*).

Quench-Flow Analysis. Quench-flow experiments were carried out with a KinTek RQF-3 rapid quench-flow instrument as previously described (*10*). All reaction components were dissolved in 100 mM Tris-HCl buffer at pH 8.3. A

Table 1: Ligand-Binding Properties of Wild-Type HPPK and the Mutants

	wild type	R84A	W89A
$K_{d(MgAntATP)}$ (μM)	1.6 ± 0.05	2.6 ± 0.2	3.6 ± 0.3
$K_{d(MgATP)}$ (μM)	2.6 ± 0.06[a]	4.2 ± 0.1	7.6 ± 0.2
$K_{d(MgAMPCPP)}$ (μM)	0.077 ± 0.006[b]	0.046 ± 0.002	0.23 ± 0.01
$K_{d(HP)}$ (μM)	0.17 ± 0.01[b]	0.22 ± 0.003	1.1 ± 0.02

[a] From Shi et al. (*7*). [b] From Li et al. (*10*).

trace amount of [α-^{32}P]ATP was used to follow the reactions. The reactions were initiated with Mg^{2+} at 30 °C and quenched with 500 mM EDTA. The substrates and products were separated by thin-layer chromatography on a plastic sheet coated with PEI-cellulose developed with 0.25 M NaH_2PO_4. The radioactivity was quantified by a Molecular Dynamics Storm 820 Phosphor-Imager. The reaction mixture contained 10 μM mutant enzyme, 100 μM ATP, 55−275 μM HP, 25 mM DTT, 0.5 mM EDTA, and 10 mM $MgCl_2$ in 100 mM Tris-HCl buffer at pH 8.3. The presteady-state data were first analyzed by a nonlinear least-squares fit of the data to eq 1.

$$[\mathrm{AMP}]/[\mathrm{HPPK}] = A(1 - e^{-\lambda t}) + k_{\mathrm{cat}}t \quad (1)$$

The burst phase is characterized by two constants, the amplitude A and the rate constant λ. The steady-state phase is characterized by the rate constant k_{cat}. The three constants are related to the rate constants in Figure 1b according to the following equations (*18*).

$$A = \frac{k_3(k_3 + k_{-3})}{(k_3 + k_{-3} + k_4)^2} \quad (2)$$

$$\lambda = k_3 + k_{-3} + k_4 \quad (3)$$

$$k_{\mathrm{cat}} = \frac{k_3k_4}{k_3 + k_{-3} + k_4} \quad (4)$$

The amplitude and rate constants for the two phases of the reaction were evaluated by a nonlinear least-squares fit to eq 1. The individual rate constants were then estimated according to eqs 2−4. These rate constants were then used along with those obtained by the stopped-flow measurements to set the initial values for the least-squares fit by numerical analysis using DYNAFIT (*17*), as previously described (*10*). The kinetic model for the numerical analysis is depicted in Figure 1b, and the goodness of the least-squares fit was judged by the χ^2 value and residual distribution.

Crystallization and Structure Determination. Apo W89A and its ternary complex with MgAMPCPP and HP (W89A·MgAMPCPP·HP) were crystallized at room temperature (19 ± 1 °C) using the hanging-drop vapor-diffusion technique. The drops were formed by mixing equal volumes of protein and reservoir solutions (Table 3). Crystals of apo W89A appeared after 2 days, and after about 3 weeks, they grew to the size suitable for data collection. Crystals of W89A·MgAMPCPP·HP appeared after 3 days, and in about 3 weeks, they grew to the size suitable for X-ray diffraction (Table 3).

X-ray diffraction data were collected at cryogenic temperature (100 K), with an ADSC Quantum-4 CCD detector mounted at the synchrotron beamline X9B at the National Synchrotron Light Source, Brookhaven National Laboratory. The apo W89A crystal belongs to space group $P2_1$ with unit-cell parameters a = 36.13 Å, b = 46.57 Å, c = 43.37 Å, and β = 110.37°. The ternary complex W89A·MgAMPCPP·HP crystal is also monoclinic, $P2_1$, with a = 47.99 Å, b = 47.39 Å, c = 71.44 Å, and β = 104.13°. Data processing was carried out with the HKL2000 program suite (*19*). The details of data collection are summarized in Table 4. The crystal structures were solved using the molecular replacement program AMoRe (*20*). The search model for apo W89A was the 1.5 Å structure of apo HPPK [PDB accession code 1HKA (*3*)], and that for the ternary complex was the 1.25 Å structure of HPPK·MgAMPCPP·HP [PDB accession code 1Q0N (*6*)]. Solvent molecules and ligands were removed from the search models. The initial refinement was carried out with the simulated annealing methods using CNS (*21*). All graphics work, including model building and rebuilding, was carried out with O (*22*).

Both structures were refined with anisotropic temperature factors for non-hydrogen atoms, excluding those in regions with highly increased mobility. Hydrogen atoms of the protein and cofactors were built geometrically at their idealized positions and assigned isotropic thermal parameters equal to 1.2 times the equivalent isotropic thermal parameters of their parent atoms. Positional parameters of ligands and ions have been refined with geometric restrictions for bond lengths, valence angles, and planarity. The geometry of finalized structures was assessed using PROCHECK (*23*). The details of refinement and the statistics of final structures are summarized in Table 4.

RESULTS

Thermodynamic Analysis. To investigate the roles of R84 and W89 in the catalysis of HPPK, we replaced the two residues, separately, by alanine. Our biochemical characterization of the mutants began with the equilibrium measurements of the binding properties of the mutants following the thermodynamic and kinetic framework for the reaction (Figure 1b) that we established earlier (*10*). We first determined the K_d values of MgAnt-ATP, a fluorescent analogue of MgATP by fluorometric titration. The K_d values of other nucleotides were then determined by a competitive binding assay measuring the fluorescent changes caused by the displacement of MgAnt-ATP by the other nucleotides (Figure 3a). The dissociation constants of HP were measured in the presence of MgAMPCPP, an MgATP analogue and dead-end inhibitor (Figure 3b), because the HPPK-catalyzed reaction apparently follows an ordered mechanism (Figure 1b) (*10*, *24*). The results of the thermodynamic analysis are summarized in Table 1. For the mutant R84A, all of the measured K_d values were comparable with those for the wild type. Of W89A, the K_d values for the nucleotides were 2−3 times those of the wild type, whereas the K_d value for HP was 6.5 times that of wild-type HPPK.

Transient Kinetic Analysis. Because a mutation can alter the rate constants for the binding of a ligand without altering its dissociation constant as we observed for the mutant R92A (*11*), we determined the rate constants for the binding of the substrates or substrate analogues for the mutant proteins. The rate constants for the binding of MgATP could be

Table 2: Kinetic Parameters of Wild-Type HPPK and the Mutants

	wild type[a]	wild type*[b]	R84A	W89A
k_1 (μM^{-1} s^{-1})	0.27 ± 0.001		0.53 ± 0.002	
	0.3 ± 0.02[c]		0.24 ± 0.02[c]	0.25 ± 0.01[c]
k_{-1} (s^{-1})	0.95 ± 0.001		1.4 ± 0.002	
	0.023 ± 0.002[c]		0.012 ± 0.002[c]	0.053 ± 0.002[c]
k_2 (μM^{-1} s^{-1})	11 ± 0.03		7.3 ± 0.02	13 ± 0.5
k_{-2} (s^{-1})	2.0 ± 0.04		2.1 ± 0.004	12 ± 0.6
k_3 (s^{-1})	16 ± 1	25 ± 2	6.3 ± 0.53[d]	1.1 ± 0.1[d]
k_{-3} (s^{-1})	20 ± 1	27 ± 4	17 ± 1[d]	0.81 ± 0.09[d]
k_4 (s^{-1})	1.8 ± 0.1	1.3 ± 0.1	1.2 ± 0.1[d]	0.70 ± 0.08[d]
k_{cat} (s^{-1})	0.76	0.61	0.31[d]	0.29[d]

[a] From Li et al. (*10*). [b] WT*, wild-type HPPK with four extra residues Gly-Ser-His-Met at the N terminus. [c] Measured for MgAMPCPP, this paper. [d] Measured for R84A* and W89A* with four extra residues Gly-Ser-His-Met at the N terminus.

Table 3: Crystallization of Apo W89A and Ternary Complex W89A·MgAMPCPP·HP

	apo W89A	W89A·MgAMPCPP·HP
protein solution		
protein (mg/mL)	10	9
AMPCPP (mM)		25
HP (mM)		15
$MgCl_2$ (mM)	50	50
buffer	10 mM Tris-HCl at pH 8.0	10 mM Tris-HCl at pH 8.0
reservoir solution		
PEG 4000 (%, w/v)	30	30
sodium acetate (M)	0.2	
ammonium acetate (M)		0.2
$MgCl_2$ (mM)	50	
imidazole (mM)	20	
buffer	0.2 M Tris-HCl at pH 8.4	0.1 M sodium acetate at pH 4.6
crystal		
shape	thin plate	block
dimensions (mm^3)	$0.001 \times 0.20 \times 0.30$	$0.15 \times 0.20 \times 0.25$
number of molecules/asymmetric unit	1	2

Table 4: Summary of X-ray Diffraction Data, Structure Solution, and Refinement

	apo W89A	W89A·MgAMPCPP·HP
X-ray diffraction data		
space group	$P2_1$	$P2_1$
resolution (Å)	1.45	1.25
number of measured reflections	97 445	347 157
number of unique reflections	23 408	85 986
completeness (%), overall/last shell	97.7/95.8	99.8/99.3
R_{merge}, overall/last shell	0.060/0.630	0.078/0.602
$I/\sigma(I)$, overall/last shell	19.4/1.9	16.8/2.0
molecular replacement		
search model (PDB code)	1HKA	1Q0N
correlation coefficient	0.67	0.58
R factor	0.35	0.42
refinement and statistics		
number of data for refinement	22 205	81 812
number of data for R_{free}	1188	4128
number of residues/non-H atoms	158/1350	316/2557
number of heterogeneous atoms	3	126
number of water oxygen atoms	252	655
final R_{free}	0.174	0.165
final *R* factor	0.155	0.132
rmsd (Å)		
bond lengths	0.014	0.012
bond angles	0.032	0.029
estimated coordinate error	0.193	0.137
overall B_{iso} ($Å^2$)	24.1	16.7
Wilson *B* factor ($Å^2$)	21.3	14.4
Ramachandran statistics (%)		
most favored φ/ψ values	92.6	91.9
disallowed φ/ψ values	0	0

measured for R84A by monitoring a small but significant change in the protein fluorescence attributed to W89. There was little change in the protein fluorescence upon the binding of MgATP. However, a dramatic change in the fluorescence was observed upon HP binding. Therefore, the binding of HP could be measured by stopped-flow fluorometry. To

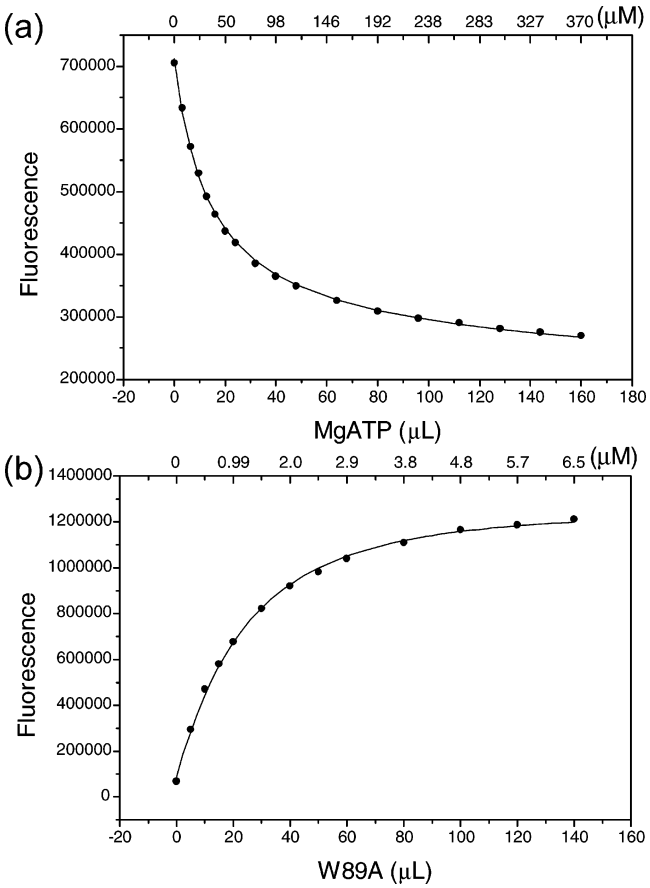

FIGURE 3: Thermodynamic analysis of the binding of MgATP (a) and HP (b) to W89A. (a) Solution containing 10 μM W89A and 10 μM Ant-ATP in 100 mM Tris-HCl and 10 mM $MgCl_2$ at pH 8.3 was titrated with ATP at 24 °C. The concentration of the ATP stock solution was 5.0 mM. The top axis indicates the concentrations of ATP during the titration. (b) Solution containing 0.55 μM HP and 100 μM AMPCPP in 100 mM Tris-HCl, 10 mM $MgCl_2$, and 25 mM DTT at pH 8.3 was titrated with W89A at 24 °C. The concentration of the W89A stock solution was 100 μM. The top axis indicates the concentrations of the mutant protein during the titration. The solid lines in both panels were obtained by nonlinear least-squares analysis.

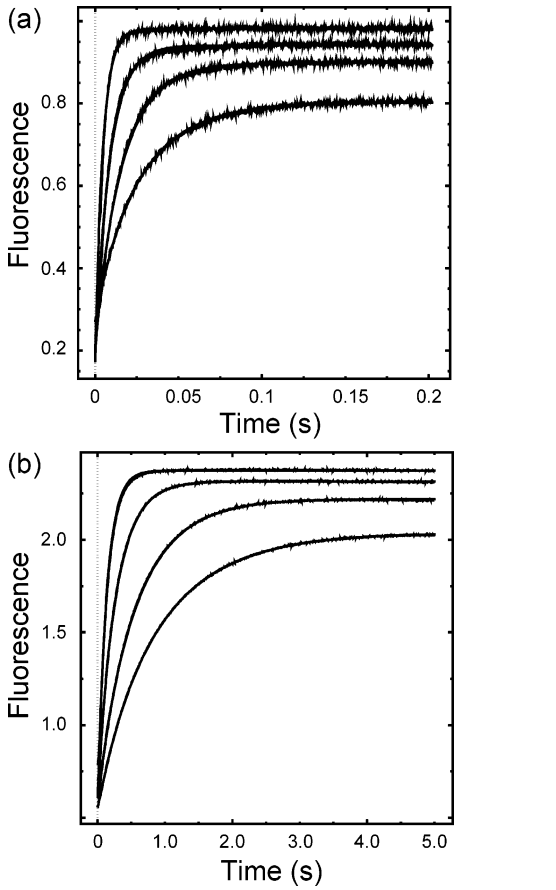

FIGURE 4: Stopped-flow analysis of the binding of MgAMPCPP (a) and HP (b) to W89A. (a) Concentrations of HP, AMPCPP, and $MgCl_2$ were fixed at 1 μM, 30 μM, and 10 mM, respectively. The concentrations of W89A were 2, 4, 8, and 16 μM for traces from the bottom to the top, respectively. (b) Concentrations of W89A, HP, and $MgCl_2$ were fixed at 1 μM, 20 μM, and 10 mM, respectively. The concentrations of AMPCPP were 5, 7.5, 15, and 30 μM for traces from the bottom to the top, respectively. All concentrations refer to the concentrations right after the rapid mixing. The solid lines were obtained by global fitting using DYNAFIT (*17*).

avoid the chemical reaction, the kinetics of the binding of HP was measured in the presence of MgAMPCPP instead of MgATP (Figure 4a). The protein was preincubated with an excess of MgAMPCPP in one syringe and then mixed with HP. Because the binding of MgAMPCPP and HP follows an ordered process with MgAMPCPP binding first, the fluorescent change reflected the kinetics of HP binding. On the other hand, when HPPK was mixed with MgAMPCPP and HP at the same time, the fluorescent change reflected mainly the kinetics of the binding of MgAMPCPP. Because we already measured the rate constants for the binding of HP, we could precisely measure the rate constants for the binding of MgAMPCPP in the presence of excess HP by monitoring the fluorescence change of HP (Figure 4b).

The catalytic properties of the mutants were measured by quench-flow analysis. Because the *E. coli* strain BL21(DE3) used to produce the mutant proteins contained a wild-type gene for HPPK in its chromosome and the same procedure was used to purify the wild-type and the mutant proteins, the protein preparations of the mutants contained a minute amount of the wild-type protein, estimated to be <0.1% based on the levels of the expression of the genes. The minute contamination of the wild-type protein did not have any significant effects on the measurements of the ligand-binding properties of the mutants, but it might have significant effects on the kinetic measurement as we observed earlier for other mutants (*11*).

To eliminate the contamination of wild-type HPPK, we fused the mutant genes in frame to the gene-encoding GST. The fusion proteins were purified by affinity chromatography with a glutathione agarose column, thus eliminating the wild-type HPPK produced by the chromosomal gene. The GST moiety was removed by thrombin cleavage, leaving the protein with four extra residues Gly-Ser-His-Met at the N terminus indicated by an asterisk (the N-terminal methionine is removed in the native HPPK). The results of the quench-flow analysis along with that of the wild-type HPPK* are shown in Figure 5. The time course of either mutant consists of two phases as that of the wild-type HPPK*, a burst phase and a steady-state phase as described by eq 1. The values for the individual rate constants of wild-type HPPK and the mutants obtained by a nonlinear least-squares fit and numerical analysis are listed in Table 2. The k_{cat} values were calculated according to eq 4 and are also listed in Table 2.

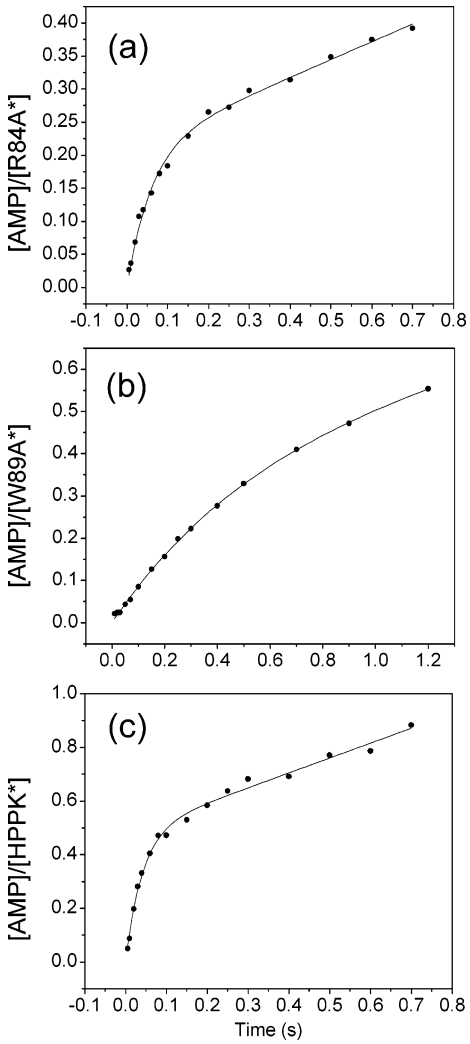

FIGURE 5: Quench-flow analysis of R84A* (a), W89A* (b), and HPPK* (c). The asterisks indicate four extra residues Gly-Ser-His-Met at the N termini of the enzymes. The reaction mixture contained 10 μM enzyme (HPPK* or the mutants), 100 μM ATP, 110 μM HP, 25 mM DTT, 0.5 mM EDTA, and 10 mM $MgCl_2$ in 100 mM Tris-HCl buffer at pH 8.3. The reaction was initiated by mixing with $MgCl_2$ at 30 °C and quenched by mixing with EDTA. The solid lines were obtained by nonlinear least-squares fit to eq 4 as described under the Experimental Procedures.

The effects of both mutations on the catalytic properties are moderate, and both mutants still showed burst kinetic behaviors (Figure 5). The R84A caused a decrease in the rate constant for the forward reaction (k_3) and k_{cat} by a factor of 3 and 2, respectively; the other kinetic constants (k_{-3} for the reverse reaction and k_4 for product release) are comparable with those of wild-type HPPK. The W89A mutation caused a decrease in k_3, k_{-3}, k_4, and k_{cat} by a factor of 15, 25, 3, and 2, respectively. Although the two single mutations caused the decrease of k_{cat} by a factor of 2, W89A altered almost all catalytic steps significantly, which might be related to the structural perturbations resulted from this mutation.

Crystal Structures of the W89A Mutant. The structure of the apo W89A was determined at 1.45-Å resolution. The structure of the mutant is very similar to that of the wild type except for three regions, loop 2 (residues 43−53), loop 3 (82−92), and the C-terminal region residues 150−155 (Figure 6). When these regions are excluded, the root-mean-square deviation (rmsd) between the Cα atoms of the apo wild-type (*3*) and mutant structures is only 0.34 Å. The rmsd values of the three regions are 2.3, 5.8, and 3.3 Å for loop 2, loop 3, and the C-terminal region, respectively. The conformational change of loop 3 makes the apo W89A structure more open than apo HPPK (Figure 6).

The structure of the ternary complex of W89A (W89A·MgAMPCPP·HP) was determined at 1.25-Å resolution (Figure 7a). The asymmetric unit contains two independent molecules, Mol A and Mol B. The conformations of the two molecules are essentially the same except for several residues in loops 2 and 3. Both molecules are superimposed well with the ternary complex of the wild type [HPPK·MgAMPCPP·HP, PDB code 1Q0N (*6*)] (Figure 7a). Only residues 46−49, 83−91, 149, and 150 have rmsd values higher than 1.0 Å between the mutant and wild-type molecules. When residues 46−49, 83−91, 149, and 150 are excluded, the Cα rmsd of the rest of the enzyme is 0.32 Å between Mol A of the mutant complex and the wild-type complex and 0.30 Å between Mol B of the mutant complex and the wild-type complex. The rmsd of the Cα atoms of residues 83−91 between the wild-type and mutant ternary complex structures is quite high, 4.4 Å between Mol A and the wild-type complex and 4.3 Å between Mol B and the wild-type complex. Despite the significant conformational changes in loop 3, the positions of the bound substrate HP, the ATP analogue AMPCPP, and two Mg^{2+} ions are the same in the structures of the two ternary complexes (Figure 7). The interactions between the enzyme and the bound ligands are illustrated in Figure 7b and listed in Table 5. In addition to the expected loss of the interactions between W89 and the bound ligands, the interactions between R84 and the nucleotide are also lost because of the conformational change of loop 3. The mutant complex, however, gains a few new interactions with the nucleotide involving the side chains of R82 and K88 and the main-chain amide of A86. The interaction between the NH group at position 8 of HP and the main-chain carbonyl of L45 is weakened, with the distance between the N and O lengthened from 2.9 to 3.7 Å.

DISCUSSION

By deletion mutagenesis, we have shown that loop 3 is essential for HPPK catalysis. A shortening of the loop by six residues caused an increase in the dissociation constant of HP by a factor of ~100 and a decrease in the rate constant for the chemical step by a factor of $\sim 1.1 \times 10^5$. The deletion mutation, however, also removed R84 and W89 that have hydrogen bond and other interactions with the substrates according to the crystal structures of the ternary complexes (*5*, *6*) (Figure 2). Thus, it is not certain whether the functional importance of the loop is due to the interactions of the side-chain groups of R84 and W89 on the loop with the substrates or the loop itself. The roles of the two residues in HPPK catalysis are investigated in this paper.

The guanidinium group of R84 forms two moderate hydrogen bonds with AMPCPP in HPPK·MgAMPCPP·HP (*6*) (Figure 2a) and two strong hydrogen bonds with ATP in the HPPK·MgATP·HP analogue (*5*) (Figure 2b). However, substitution of R84 with alanine causes minimal changes in either the dissociation constants (Table 1) or kinetic constants of the HPPK-catalyzed reaction, except the rate constant for

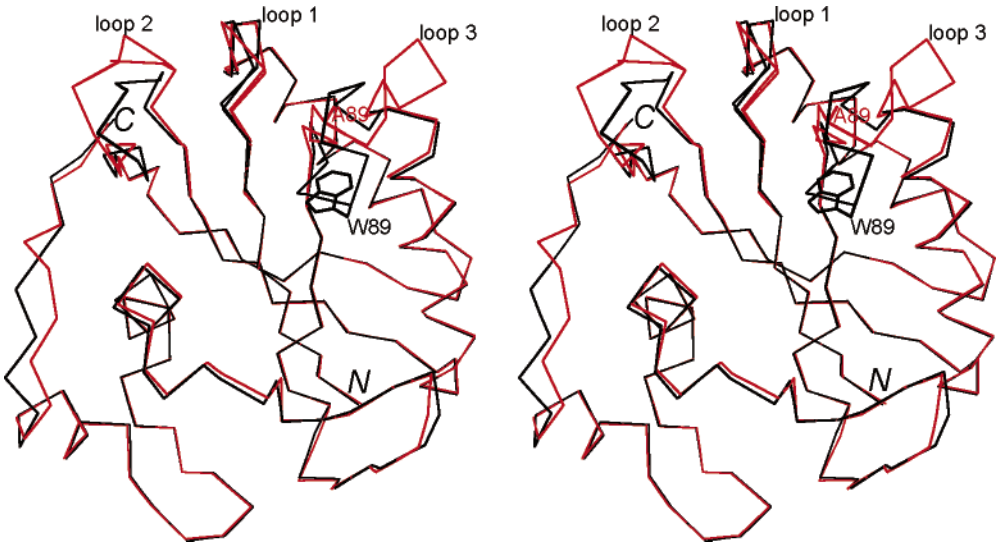

FIGURE 6: Stereoview of the superposition of the apo W89A and the wild-type apo HPPK. The Cα trace of apo W89A (this paper) is in red, and that of apo HPPK [PDB accession code 1HKA (*5*)] is in black. The figure was prepared with MolScript (*25*).

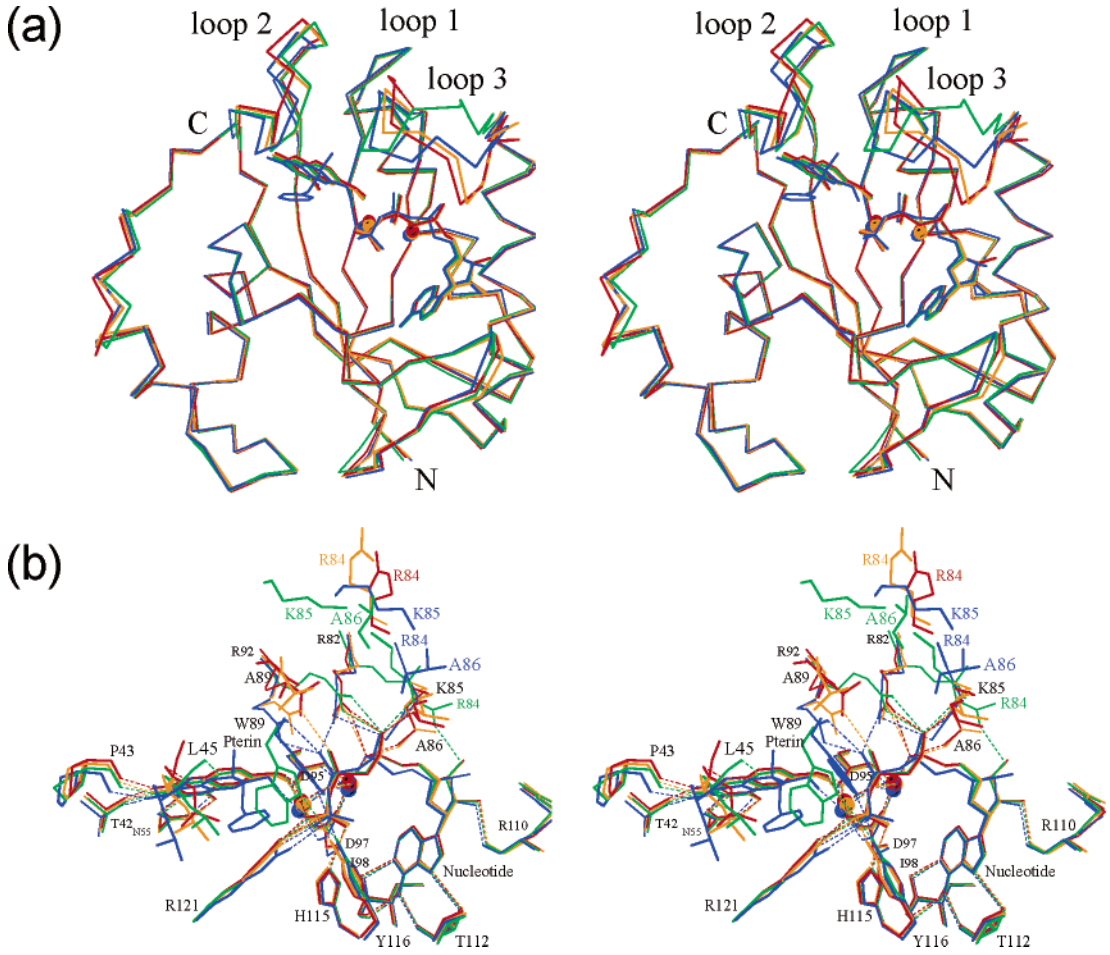

FIGURE 7: Stereoview showing the comparison between the ternary complexes of W89A and wild-type HPPK. (a) Superposition of the Cα traces of HPPK·MgAMPCPP·HP (*6*) (green), HPPK·MgATP·HP analogue (*5*) (blue), Mol A (red), and Mol B (orange) of W89A·MgAMPCPP·HP (this paper). The bound substrates and substrate analogues are also shown in the same color scheme as for the Cα traces. (b) Polar interactions between the enzyme and the substrate and substrate analogue in HPPK·MgAMPCPP·HP (green), HPPK·MgATP·HP analogue (blue), MolA (red), and MolB (orange) of W89A·MgAMPCPP·HP. The bound Mg^{2+} ions are shown as solid spheres. The covalent bonds are in solid lines, and the hydrogen bonds and Mg^{2+} coordinations are in dotted lines. The labels are in the same color scheme as that for the structures except that black labels are used for residues of two or more structures for clarity. The figure was prepared with MolScript (*25*).

the chemical step of the forward reaction (k_3) and k_{cat} (Figure 1b and Table 2), which decrease by a factor of only 3 and 2, respectively. The results indicate that despite the hydrogen bonds of the guanidinium group of R84 to MgATP, R84 is dispensable for the binding of substrates and plays only a very minor role in catalysis.

Table 5: Polar Interactions between the Enzyme and the Bound Substrate or Substrate Analogues

interactions	distance (Å)			
	1Q0N[a]	1DY3[a]	Mol A[a]	Mol B[a]
pterin-N1:L45-N	3.0	3.12	3.13	2.98
pterin-N2:P43-O	2.84	2.94	2.80	2.77
pterin-N2:T42-OG1	2.83	2.76	2.81	2.79
pterin-N3:N55-OD1	2.98	2.91	2.84	2.89
pterin-O4:N55-ND2	2.76	2.81	2.81	2.80
pterin-N8:L45-O	2.94	2.77	3.73	3.74
pterin-O6:D95-OD2	2.87	3.89	2.87	2.92
nucleotide-O1G:H115-NE2	3.09		3.05	3.35
nucleotide-O2G:Y116-OH	2.60	2.41	2.62	2.70
nucleotide-O2G:W89-NE1	2.82	3.18		
nucleotide-O2G:R121-NH2	2.80	3.01	2.72	2.81
nucleotide-O3G:R121-NH1	2.89	2.73	2.88	2.85
nucleotide-O2B:R92-NH1	3.41	2.98	2.95	3.02
nucleotide-O2B:R92-NH2	3.61	2.91	4.33	3.15
nucleotide-O2B:R82-NH2		3.19		
nucleotide-O2A:R92-NH1	3.10			
nucleotide-O2A:R92-NH2	2.99			
nucleotide-O2A:R82-NH2		3.27	3.05	3.12
nucleotide-O2A:R84-NE	3.20	2.60		
nucleotide-O2A:A86-N			2.80	2.85
nucleotide-O1A:R82-NH2		3.08	2.99	3.11
nucleotide-O1A:R84-NH2		2.45		
nucleotide-O1A:R92-NH1	3.18			
nucleotide-O1A:K85-NZ			2.94	2.90
nucleotide-O3*:R84-NH2	2.98			
nucleotide-O2*:R110-O	2.60	2.49	2.64	2.63
nucleotide-N1:I98-N	2.95	3.05	3.00	2.97
nucleotide-N6:I98-O	2.76	2.83	2.75	2.76
nucleotide-N6:T112-O	3.07	2.97	3.08	2.98
nucleotide-N7:T112-N	3.04	3.00	2.97	3.02

[a] 1Q0N, 1DY3, Mol A, and Mol B stand for HPPK·MgAMPCPP·HP (*6*), HPPK·MgATP·HP analogue (*5*), and Mol A and Mol B of W89A·MgAMPCPP·HP (this paper), respectively.

Substitution of W89A with alanine decreases the K_d value for the binding of MgATP and HP by a factor of 3 and 6, respectively, indicating that the indole ring of W89 makes some minor contributions to the binding of the substrates. The larger effects of the W89A mutation are a decrease on the rate constant for the chemical step of the forward reaction by a factor of 15 and on the rate constant for the reverse reaction by a factor of 25, suggesting a moderate role of W89 in the transition-state stabilization.

The structure of apo W89A is very similar to that of apo wild-type HPPK except in three regions: loops 2 and 3 and the C-terminal region residues 150−155 (Figure 6). Loops 2 and 3 are long loops and are rather flexible when the enzyme is in the apo form, as evidenced by their high-temperature factors in the crystal structure and low intensities in the ^{1}H-^{15}N HSQC spectrum (*3*). The apo structures of other mutants also show significantly different conformations in the two loops and the C-terminal region (*12*). The conformational changes in these regions probably reflect the inclination of these regions to adopt different conformations rather than the consequences of removing certain interactions by the mutations, because the indole ring of W89 is at the surface with minimal interactions with the other residues of loop 3 and no interactions with the rest of the HPPK molecule.

The structure of the ternary complex of W89A with HP and AMPCPP is more similar to that of the ternary complex of wild-type HPPK (Figure 7a) than the structure of the apo W89A to that of the wild-type apo HPPK (Figure 6). However, the conformation of loop 3 is quite different from that of the wild-type HPPK·MgAMPCPP·HP, and less so is the conformation of loop 2. The conformational differences of the loops cause several differences in the interactions between the substrate and substrate analogue with the enzyme, as described in the Results, summarized in Table 5, and illustrated in Figure 7b. In the W89A·MgAMPCPP·HP complex, the guanidinium group of R84 does not interact with the nucleotide. Instead, it points away from the substrate-binding site (Figure 7b). However, the loss of the hydrogen-bond interactions between the nucleotide and R84 is insignificant, because the R84A mutation causes little functional consequences and it may also be compensated by the interactions with the side chain of K85 and the main chain of A86 gained by the new loop conformation. The weakening of the hydrogen bond between N8 of HP and the carbonyl of L45 may be responsible for the weaker binding of HP by W89A. Most importantly, the guanidinium groups of the two catalytic residues R82 and R92 interact with the β and γ phosphate of the nucleotide, where the bond cleavage and formation occurs (Figure 7b). The conformations of the two guanidinium groups are very similar to those observed in the structure of the HPPK·MgATP·HP analogue (*5*). We also observed such arrangements in a 0.89-Å crystal structure of a ternary complex of wild-type HPPK (*12*). Thus, the conformation of loop 3 in W89A·MgAMPCPP·HP represents a conformation competent for catalysis. In contrast, the guanidinium groups of both R82 and R92 in the crystal structure of the ternary complex of the deletion mutant point away from the active center, which essentially abolished the catalytic activity (*13*). The biochemical and structural results of the two mutants clearly show that the essential role of loop 3 in catalysis is not due to the interactions of R84 and W89 with the substrate but rather due to the loop itself, which is required for the positioning of the two catalytic residues R82 and R92 for catalysis (*13*).

ACKNOWLEDGMENT

We thank Dr. Z. Dauter for his help during the X-ray data acquisition at the synchrotron beamline X9B of the NSLS, Brookhaven National Laboratory. J. B. would like to thank J. L. Brooks for critical discussion and continuous encouragement.

REFERENCES

1. Shiota, T. (1984) Biosynthesis of folate from pterin precursors, in *Chemistry and Biochemistry of Folates* (Blakley, R. T., and Benkovic, S. J., Eds.) pp 121−134, John Wiley and Sons, New York.
2. Blakley, R. L., and Benkovic, S. J. (1984) in *Folates and Pterins*, John Wiley and Sons, New York.
3. Xiao, B., Shi, G., Chen, X., Yan, H., and Ji, X. (1999) Crystal structure of 6-hydroxymethyl-7,8-dihydropterin pyrophosphokinase, a potential target for development of novel antimicrobial agents, *Structure 7*, 489−496.
4. Hennig, M., Dale, G. E., D'Arcy, A., Danel, F., Fischer, S., Gray, C. P., Jolidon, S., Müller, F., Page, M. G. P., Pattison, P., and Oefner, C. (1999) The structure and function of the 6-hydroxymethyl-7,8-dihydropterin pyrophosphokinase from *Haemophilus influenzae*, *J. Mol. Biol. 287*, 211−219.
5. Stammers, D. K., Achari, A., Somers, D. O., Bryant, P. K., Rosemond, J., Scott, D. L., and Champness, J. N. (1999) 2.0 Å X-ray structure of the ternary complex of 7,8-dihydro-6-hydroxymethylpterin pyrophosphokinase from *Escherichia coli* with ATP and a substrate analogue, *FEBS Lett. 456*, 49−53.

6. Blaszczyk, J., Shi, G., Yan, H., and Ji, X. (2000) Catalytic center assembly of 6-hydroxymethyl-7,8-dihydropterin pyrophosphokinase as revealed by the crystal structure of a ternary complex at 1.25 Å resolution, *Structure 8*, 1049−1058.
7. Shi, G., Gong, Y., Savchenko, A., Zeikus, J. G., Xiao, B., Ji, X., and Yan, H. (2000) Dissecting the nucleotide binding properties of *Escherichia coli* 6-hydroxymethyl-7,8-dihydropterin pyrophosphokinase with fluorescent 3′(2)′-*O*-anthraniloyladenosine 5′-triphosphate, *Biochim. Biophys. Acta 1478*, 289−299.
8. Shi, G. B., Blaszczyk, J., Ji, X. H., and Yan, H. G. (2001) Bisubstrate analogue inhibitors of 6-hydroxymethyl-7,8-dihydropterin pyrophosphokinase: Synthesis and biochemical and crystallographic studies, *J. Med. Chem. 44*, 1364−1371.
9. Xiao, B., Shi, G., Gao, J., Blaszczyk, J., Liu, Q., Ji, X., and Yan, H. (2001) Unusual conformational changes in 6-hydroxymethyl-7,8-dihydropterin pyrophosphokinase as revealed by X-ray crystallography and NMR, *J. Biol. Chem. 276*, 40274−40281.
10. Li, Y., Gong, Y., Shi, G., Blaszczyk, J., Ji, X., and Yan, H. (2002) Chemical transformation is not rate-limiting in the reaction catalyzed by *Escherichia coli* 6-hydroxymethyl-7,8-dihydropterin pyrophosphokinase, *Biochemistry 41*, 8777−8783.
11. Li, Y., Wu, Y., Blaszczyk, J., Ji, X., and Yan, H. (2003) Catalytic roles of arginine residues 82 and 92 of *Escherichia coli* 6-hydroxymethyl-7,8-dihydropterin pyrophosphokinase: Site-directed mutagenesis and biochemical studies, *Biochemistry 42*, 1581−1588.
12. Blaszczyk, J., Li, Y., Shi, G., Yan, H., and Ji, X. H. (2003) Dynamic roles of arginine residues 82 and 92 of *Escherichia coli* 6-hydroxymethyl-7,8-dihydropterin pyrophosphokinase: Crystallographic studies, *Biochemistry 42*, 1573−1580.
13. Blaszczyk, J., Li, Y., Wu, Y., Shi, G., Ji, X. H., and Yan, H. (2004) Essential roles of a dynamic loop in the catalysis of 6-hydroxymethyl-7,8-dihydropterin pyrophosphokinase, *Biochemistry 43*, 1469−1477.
14. Blaszczyk, J., Shi, G., Li, Y., Yan, H., and Ji, X. H. (2004) Reaction trajectory of pyrophosphoryl transfer catalyzed by 6-hydroxymethyl-7,8-dihydropterin pyrophosphokinase, *Structure 12*, 467−475.
15. Thijssen, H. H. W. (1973) A simple method for preparing 2-amino-4-hydroxy-6-formylpteridine, a precursor of the pteridine substrate of dihydropteroate biosynthesis, *Anal. Biochem. 54*, 609−611.
16. Scrimgeour, K. G. (1980) Methods for reduction, stabilization, and analyses of folates, *Methods Enzymol. 66*, 517−523.
17. Kuzmic, P. (1996) Program DYNAFIT for the analysis of enzyme kinetic data: Application to HIV proteinase, *Anal. Biochem. 237*, 260−273.
18. Johnson, K. A. (1992) Transient-state kinetic analysis of enzyme reaction pathways, in *The Enzymes* (Sigman, D. S., Ed.) pp 1−61, Academic Press, San Diego, CA.
19. Otwinowski, Z., and Minor, W. (1997) Processing of X-ray diffraction data collected in oscillation mode, *Methods Enzymol. 276*, 307−326.
20. Navaza, J. (1994) An automated package for molecular replacement, *Acta Crystallogr., Sect. A 50*, 157−163.
21. Brünger, A. T., Adams, P. D., Clore, G. M., DeLano, W. L., Gros, P., Grosse-Kunstleve, R. W., Jiang, J.-S., Kuszewski, J., Nilges, N., Pannu, N. S., Read, R. J., Rice, L. M., Simonson, T., and Warren, G. L. (1998) Crystallography and NMR system (CNS): A new software system for macromolecular structure determination, *Acta Crystallogr., Sect. D 54*, 905−921.
22. Jones, T. A., and Kjeldgaard, M. (1997) Electron-density map interpretation, *Methods Enzymol. 277*, 173−208.
23. Laskowski, R. A., MacArthur, M. W., Moss, D. S., and Thornton, J. M. (1993) Procheck: A program to check the stereochemical quality of protein structures, *J. Appl. Crystallogr. 26*, 283−291.
24. Bermingham, A., Bottomley, J. R., Primrose, W. U., and Derrick, J. P. (2000) Equilibrium and kinetic studies of substrate binding to 6-hydroxymethyl-7,8-dihydropterin pyrophosphokinase from *Escherichia coli*, *J. Biol. Chem. 275*, 17962−17967.
25. Kraulis, P. J. (1991) Molscript: A program to produce both detailed and schematic plots of protein structures, *J. Appl. Crystallogr. 24*, 946−950.
26. Merritt, E. A., and Bacon, D. J. (1997) Raster3d: Photorealistic molecular graphics, *Methods Enzymol. 277*, 505−524.

BI0503495